Mon. Not. R. Astron. Soc. **360,** 1123–1131 (2005) doi:10.1111/j.1365-2966.2005.09109.x

An *XMM–Newton* observation of Mkn 3 – a Seyfert galaxy just over the edge

K. A. Pounds★ and K. L. Page
Department of Physics and Astronomy, University of Leicester, Leicester LE1 7RH

Accepted 2005 April 11. Received 2005 April 8; in original form 2005 March 15

ABSTRACT

A 100-ks *XMM–Newton* observation of the nearby Seyfert 2 galaxy Mkn 3 offers a unique opportunity to explore the complexity of its X-ray spectrum. We find the ∼3–8 keV continuum to be dominated by reflection from cold matter, with fluorescent K-shell lines detected from Ni, Fe, Ca, Ar, S, Si and Mg. At higher energies an intrinsic power-law continuum, with canonical Seyfert 1 photon index, is seen through a near-Compton-thick cold absorber. A soft excess below ∼3 keV is found to be dominated by line emission from an outflow of 'warm' gas, photoionized and photoexcited by the intrinsically strong X-ray continuum. Measured blueshifts in the strong Fe Kα and O VII and O VIII emission lines are discussed in terms of the properties of the putative molecular torus and ionized outflow.

Key words: galaxies: active – galaxies: individual: Mkn 3 – galaxies: Seyfert – X-rays: galaxies.

1 INTRODUCTION

Mkn 3 is a low-redshift, $z = 0.013\,509$ (Tifft & Cocke 1988), Seyfert 2 galaxy and one of the intrinsically brightest active galactic nuclei (AGN) above ∼10 keV (Cappi et al. 1999). However, absorption by a large column density of intervening cold matter (the torus?) results in very little of the intrinsic X-ray continuum being directly visible. Instead, previous X-ray studies with *ASCA* (Turner et al. 1997a) and *BeppoSAX* (Cappi et al. 1999) have suggested that the observed X-ray flux over the 2–10 keV band is dominated by indirect radiation 'reflected' (i.e. redirected by scattering in optically thick matter) into the line of sight. An extended soft X-ray emission component was resolved in an early *Chandra* observation (Sako et al. 2000), which also showed the soft X-ray spectrum to be dominated by blueshifted line emission from highly ionized gas. Mkn 3 is a particularly interesting object, being one of the small number of Seyfert 2 galaxies to exhibit broad optical emission lines in polarized light (Miller & Goodrich 1990; Tran 1995), while the observation of biconical [O III] emission (Pogge & de Robertis 1993; Capetti et al. 1995, 1999) also provides evidence for an extended region of ionized gas. The soft X-ray spectra of Mkn 3 have particular potential in studying an ionized outflow in Mkn 3 since it is one of the few bright Seyfert 2 galaxies not significantly 'contaminated' by starburst X-ray emission (Pogge & de Robertis 1993; Turner et al. 1997b).

In this paper we present an analysis of archival data from an early *XMM–Newton* observation of Mkn 3, which have not hitherto been published.

★E-mail: kap@leicester.ac.uk

2 OBSERVATION AND DATA REDUCTION

Mkn 3 was observed by *XMM–Newton* on 2000 October 19–20 throughout orbit 158. These data are now public and have been obtained from the *XMM–Newton* data archive. We use X-ray spectra from the EPIC pn (Strüder et al. 2001) and MOS (Turner et al. 2001) cameras, and the Reflection Grating Spectrometer (RGS; den Herder et al. 2001). Both EPIC cameras were operated in full-frame mode, together with the medium filter. The X-ray data were first screened with the SAS version 6.1 software and events corresponding to patterns 0–4 (single- and double-pixel events) were selected for the pn data and patterns 0–12 for the MOS data. EPIC source counts were taken within a circular region of 45-arcsec radius about the centroid position of Mkn 3, with the background being taken from a similar region, offset from but close to the source. The net exposures available for spectral fitting were 76.5 ks (pn), 136.5 ks (combined MOS), 105.3 ks (RGS1) and 102.0 ks (RGS2). Since no obvious variability was evident throughout the observation, spectral data were then integrated over the full exposures and binned to a minimum of 20 counts per bin, to facilitate use of the χ^2 minimalization technique in spectral fitting. Spectral fitting was based on the XSPEC package (Arnaud 1996) and all spectral fits include absorption due to the Mkn 3 line-of-sight Galactic column of $N_{\rm H} = 8.7 \times 10^{20}$ cm^{-2} (Stark et al. 1992). Errors are quoted at the 90 per cent confidence level ($\Delta\chi^2 = 2.7$ for one interesting parameter).

3 THE HARD (3–15 KEV) EPIC SPECTRUM

Fig. 1 shows the background-subtracted EPIC camera data integrated over the full observation of Mkn 3. The spectrum is seen to be highly structured and sufficiently hard to be detected to

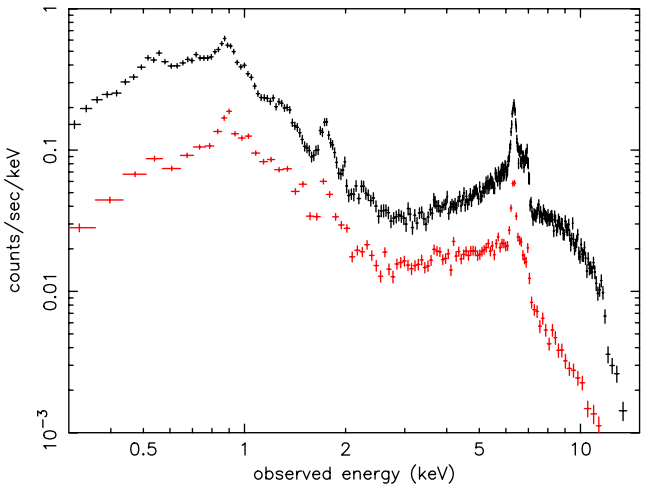

Figure 1. Background-subtracted data from the EPIC pn (black) and MOS1 (red) camera observations of Mkn 3 showing the X-ray spectrum to be detected over an unusually wide (∼0.3–15 keV) spectral band.

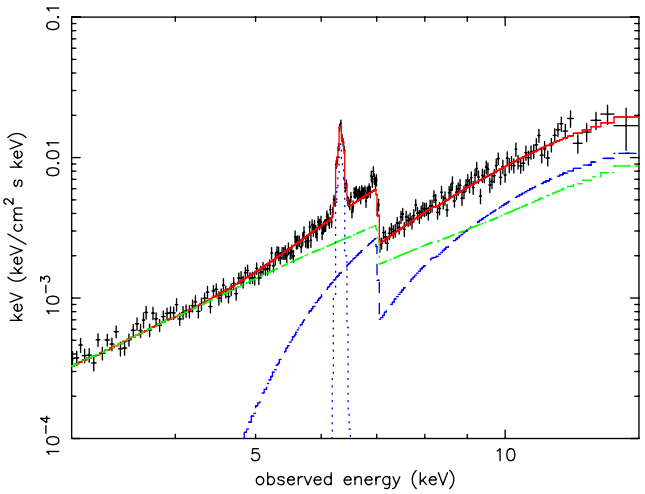

Figure 2. Unfolded model fit to the Mkn 3 EPIC spectrum $\gtrsim$3 keV, as described in Section 3, showing the absorbed power law (dark blue) plus reflection (green) components to the hard continuum and a narrow Fe Kα line (light blue). The pn camera data only are shown for clarity

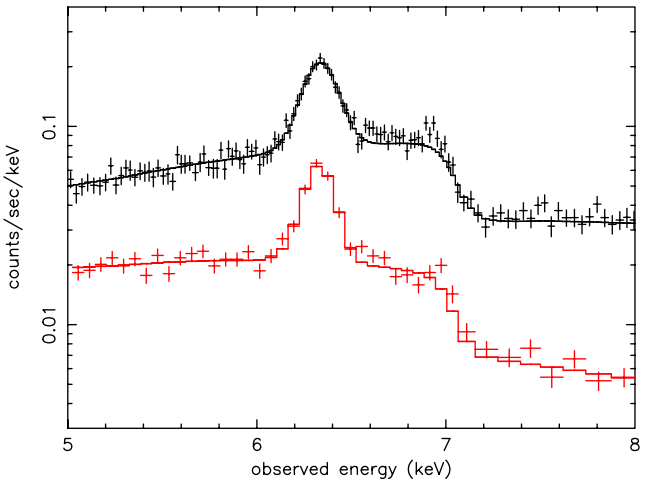

Figure 3. Comparison of the pn (black) and MOS (red) data with a power-law + reflection + Fe Kα line model, showing excess flux at ∼6.5–6.8, 7 and 7.5 keV

∼15 keV (pn) and ∼11.5 keV (MOS). Given previous reports (Sako et al. 2000) of a physically separate soft spectral component below ∼3 keV we initially restricted modelling of the EPIC spectrum to the hard X-ray (3–15 keV) band. A power-law fit above 3 keV is poor but indicates the observed spectrum to be very hard, with a photon index $\Gamma \sim -0.6$. The more complex model proposed by Turner et al. (1997a) in analysing the *ASCA* observation of Mkn 3, and adopted by Cappi et al. (1999) for their *BeppoSAX* analysis, was found to fit the data well. In that model the hard X-ray continuum is a composite of a 'canonical' Seyfert power law of photon index $\Gamma \sim 1.8$, attenuated by a near-Compton-thick absorber, and an unabsorbed reflection component. In addition the model contains an intense Fe Kα line, conceivably arising by fluorescence in the same matter responsible for the continuum reflection.

In fitting this model to the EPIC data the principal power law and Fe K line parameters were left free and untied for the pn and MOS fits. Cold reflection was modelled with PEXRAV in XSPEC (Magdziarz & Zdziarski 1995), with a reflection factor R ($= \Omega/2\pi$, where Ω is the solid angle subtended by the reflector at the continuum source) left free, but common to both pn and MOS fits. The high-energy cut-off of the incident power law was set at 200 keV (Cappi et al. 1999) and the viewing angle (to the reflector) at the default value of 60°. Element abundances were set to be solar. An excellent fit ($\chi^2 = 1327$ for 1336 degrees of freedom, dof) was obtained for a photon index of $\Gamma \sim 1.82$ (pn) and $\Gamma \sim 1.74$ (MOS), attenuated by a column of cold gas of $N_{\rm H} \sim 1.3 \times 10^{24}$ cm^{-2}. The dominant reflection continuum was represented by $R = 1.7 \pm 0.1$. The Fe Kα emission line was well fitted in the pn data by a Gaussian at 6.417 ± 0.004 keV (Mkn 3 rest-frame), of width $\sigma = 45 \pm 9$ eV and flux $= 3.8 \pm 0.3 \times 10^{-5}$ photon cm^{-2} s^{-1}. The corresponding Fe Kα line parameters from the MOS spectral fit were 6.417 ± 0.004 keV, $\sigma = 38 \pm 11$ eV and flux $4.7 \pm 0.4 \times 10^{-5}$ photon cm^{-2} s^{-1}. The line equivalent width (EW) was 600 ± 50 eV (pn) and 650 ± 55 eV (MOS) compared with the *total* local continuum. This best-fitting model for the 3–15 keV spectrum of Mkn 3 is reproduced in Fig. 2. Compared only with the reflection continuum we note that the EW of the Fe Kα line increases to 1050 ± 80 eV (pn) and 1150 ± 100 eV (MOS).

Comparing the EPIC data with the above model in the neighbourhood of the Fe Kα line (Fig. 3) reveals excess flux to higher energies, with a small peak near 7 keV. Adding a second Gaussian to the model allows one to find a narrow line at 7.07 ± 0.03 keV (AGN rest frame), with a flux of $3.2 \pm 1.8 \times 10^{-6}$ photon cm^{-2} s^{-1} and EW∼110 eV (cf. the reflection continuum), an addition which improves the fit to $\chi^2 = 1301/1333$ dof. Both the energy and relative strength are consistent with this being the Fe Kβ line, rather than Fe XXVI Lyα as proposed in the *ASCA* analysis (Turner et al. 1997a). The additional excess flux at ∼6.5–6.8 keV was then modelled by a third narrow Gaussian line, at 6.69 ± 0.05 keV (AGN rest frame) with a flux of $\sim 1.5 \times 10^{-6}$ photon cm^{-2} s^{-1} and EW∼40 eV (cf. the reflection continuum), further improving the fit to $\chi^2 = 1292/1330$ dof. We note that the energy of this emission line is close to that of He-like Fe. Finally, the small excess apparent near 7.5 keV lies close to the energy of Ni Kα emission. The addition of a fourth Gaussian gave a further small improvement to the fit ($\chi^2 = 1285/1327$ dof) with a line energy (rest frame) of 7.5 ± 0.1 keV (compared with the laboratory energy of neutral Ni Kα of 7.47 keV), a flux of $\sim 2 \times 10^{-6}$ photon cm^{-2} s^{-1} and EW ∼ 60 eV. Finally, we note that Fig. 3 shows no evident Compton shoulder on the low-energy wing of the Fe Kα line, which should occur by down-scattering when

the reprocessing matter is optically thick to electron scattering. We return to this point in the next section.

Based on the above broad-band spectral fit we find an *observed* 3–15 keV flux for Mkn 3 of 1.5×10^{-11} erg cm^{-2} s^{-1}. Correcting for the measured absorption the 3–15 keV flux increases to 4.8×10^{-11} erg cm^{-2} s^{-1}, corresponding to an *unabsorbed* luminosity of 1.9×10^{43} erg s^{-1} ($H_0 = 70$ km s^{-1} Mpc^{-1}). For later reference, extending that intrinsic power-law spectrum to 0.3 keV would give a (0.3–15 keV) luminosity of 3.3×10^{43} erg s^{-1}.

3.1 A Compton shoulder to the Fe Kα line

The absence of an obvious Compton shoulder on the low-energy wing of the strong Fe Kα line is physically inconsistent with the observed level of reprocessing either by reflection or by transmission through a near-Compton-thick absorber (Matt 2002). The width of the line is also a surprise if interpreted as being due to velocity dispersion in matter on the far inner face of the molecular torus. However, during the course of the present analysis we learned from MPE-MPG of a problem with pn counts where the photon energy is deposited in two adjacent pixels, the so-called 'doubles', whereby the registered photon energy can be ∼20 eV greater than for the same photon fully absorbed in a single pixel (K Dennerl, private communication). To test the importance of such effects on the present analysis we have repeated our fitting of the Fe Kα line using only single-pixel (pat0) counts for the pn camera.

For the pn pat0 data we initially fitted a narrow Gaussian line (i.e. with only the CCD resolution of $\sigma = 65$ eV) to the Fe Kα peak, allowing the energy and flux to be free. Fig. 4 (top) shows how

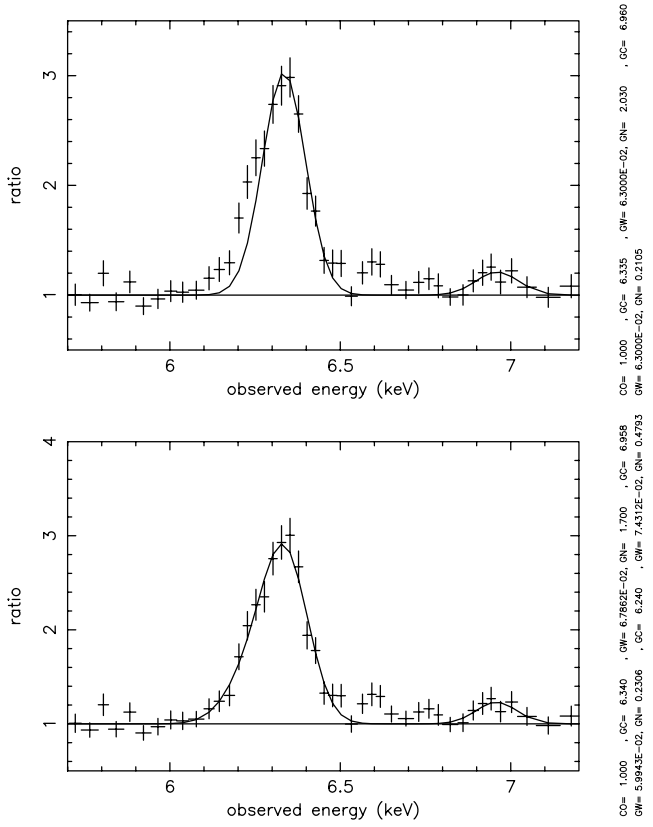

Figure 4. Gaussian lines added to the continuum model fit for the pn pat0 data. Top: narrow lines to model Fe Kα and Fe Kβ, respectively. Bottom: third Gaussian added to model the Compton scattering shoulder to the Fe Kα line. For details see Section 3.1

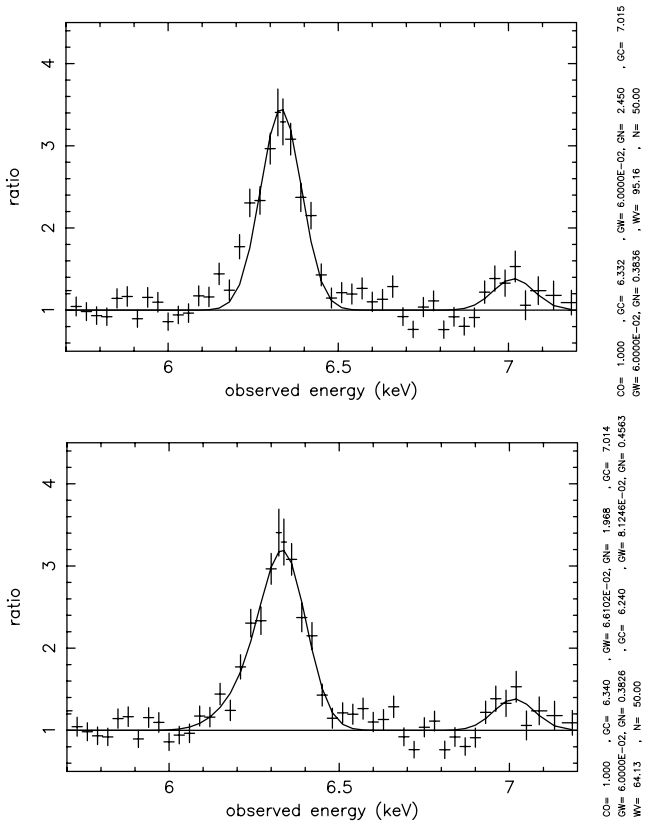

Figure 5. Gaussian lines added to the continuum model fit for the MOS data. Top: narrow lines to model Fe Kα and Fe Kβ, respectively. Bottom: third Gaussian added to model the Compton scattering shoulder to the Fe Kα line. For details see Section 3.1

the narrow line then fits the high-energy wing of the observed line while leaving an excess on the low-energy side. A second Gaussian component was then added, at an energy ∼0.1 keV lower than the Fe Kα line, as expected for single Compton scattering in cold, optically thick matter (Matt 2002), and iterated with the Fe Kα linewidth and fluxes free. While the double-Gaussian fit (Fig. 4, bottom) was statistically no improvement on the original single-Gaussian fit to the Fe Kα line, the relative strength of the Compton shoulder component to the primary Fe Kα line (∼20 per cent) now gives a physically consistent overall picture of a reflection-dominated hard X-ray spectrum for Mkn 3. The above procedure was then repeated for the MOS data, again finding an acceptable fit with a ∼23 per cent Compton component to the Fe Kα line (Fig. 5).

3.2 Fe Kα linewidth and energy

Allowing for the Compton shoulder has the important consequence that the primary Fe Kα line is now only marginally resolved, with a formal width of $\sigma = 30 \pm 15$ eV in both pn and MOS fits. However, the primary line energy is increased, and though the addition of the Compton component increases the errors, the primary line remains significantly blueshifted at 6.43 ± 0.01 eV (Mkn 3 rest-frame) for both pn pat0 and MOS data. Since fluorescent emission will be produced in the cold reflector and the nuclear absorbing column, it is reasonable to test for a common velocity with the Fe Kα line. To do so we first fixed the Fe Kα line energy at 6.40 keV, with the fit then worsening by $\Delta\chi^2 = 43$ for one additional dof. Allowing the redshift of the line in XSPEC to be free recovered the initial fit

($\chi^2 = 1285/1327$ dof), with the effective redshift falling (from $z = 0.0135$) to $(1.07 \pm 0.05) \times 10^{-2}$. Tying the redshift of the cold absorber to that of the Fe Kα line then gave a significant improvement to the 3–15 keV fit, with $\chi^2 = 1270/1327$ dof and a redshift of $(1.05 \pm 0.04) \times 10^{-2}$. Tying the redshift of the reflector to that of the line did not give a comparable improvement in the fit, though this was less well constrained. This test does suggest that a significant fraction of the Fe Kα line comes from the obscuring matter, which must then subtend a substantial solid angle to the primary source. That geometry would, in turn, offer a possible velocity-dispersion explanation for the observed linewidth.

3.3 Other spectral features in the EPIC data

Extending the above hard X-ray (3–15 keV) model fit below 3 keV reveals a marked and highly structured 'soft excess'. This excess remains (Fig. 6) after the addition of a second (unabsorbed) power-law component, with photon index fixed to the primary hard X-ray power law, intended to model any continuum scattered into the line of sight by the ionized gas responsible for the polarized optical lines in Mkn 3. The inclusion of this unabsorbed power-law component did, however, reduce the cold reflection factor to $R = 1.2 \pm 0.1$ and further improved the (3–15 keV) fit to $\chi^2 = 1270/1326$ dof. In the subsequent EPIC analysis we retain this amended 3–15 keV spectral fit.

The soft excess illustrated in Fig. 6 is found to have an *observed* flux (0.3–3 keV) of 4×10^{-13} erg cm^{-2} s^{-1}. Allowing for the significant attenuation by the Galactic column of $N_{\rm H} = 8.7 \times 10^{20}$ cm^{-2} increases this by 50 per cent, corresponding to an intrinsic soft X-ray luminosity over this energy band of 2.5×10^{41} erg s^{-1} ($H_0 = 70$ km s^{-1} Mpc^{-1}).

The reflection-dominated fit to the hard X-ray spectrum of Mkn 3 suggests that fluorescent line emission from lighter, abundant metals might be visible at lower energies, perhaps contributing to the spectral structure seen in Fig. 6. An initial examination of those pn camera data shows that the strong peaks near 2.3 and 1.8 keV lie close to the Kα line energies of S and Si, respectively. It is important to note that these features are much stronger than any calibration uncertainties associated with the Si-K and Au-M edges in the EPIC

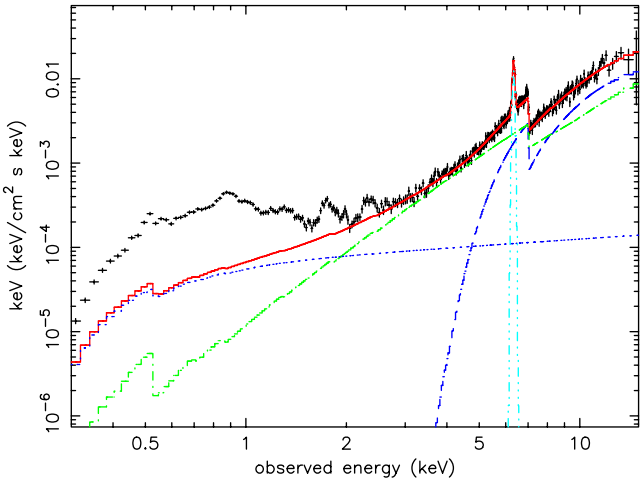

Figure 6. Low-energy extension of the 3–15 keV spectral fit, revealing a soft excess. The addition of an unabsorbed continuum component (blue dots) with photon index tied to the intrinsic power corresponds to a scattered continuum component $\leqslant 1$ per cent of this soft emission. For the sake of clarity only the pn data are shown.

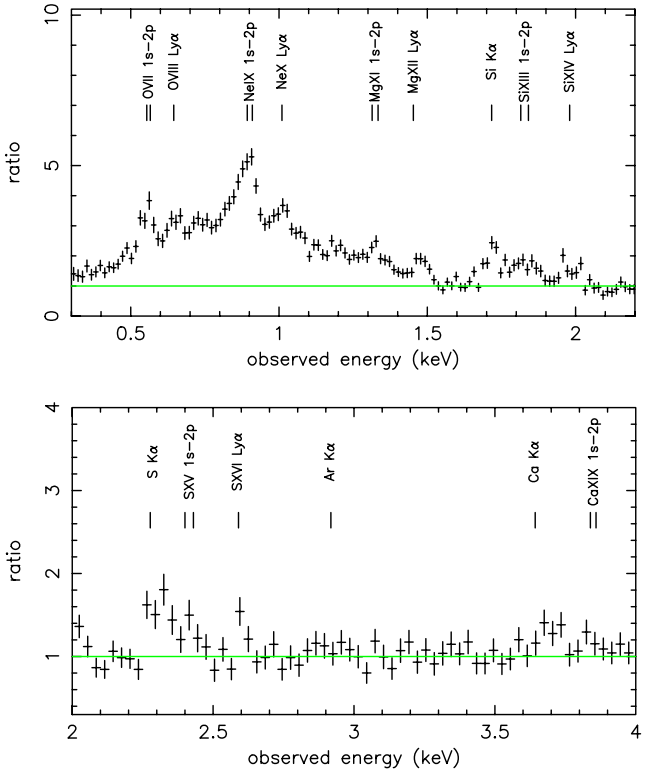

Figure 7. Identifying features in the EPIC (MOS camera) spectrum of Mkn 3 with principal emission lines: (top) of highly ionized O, Ne, Mg and Si, together with fluorescent Si Kα; (bottom) highly ionized S together with the Kα lines of S, Ar and Ca

Table 1. Candidate Kα fluorescent emission lines in the EPIC spectrum of Mkn 3. The observed line energies (keV) are adjusted to the source rest frame and compared with laboratory values. The observed equivalent widths (relative to the reflection continuum) are compared with values estimated for solar abundances and a viewing angle of 60°.

Line	$E_{\rm source}$	$E_{\rm lab}$	EW$_{\rm obs}$(eV)	EW$_{\rm est}$(eV)
Ni Kα	7.5 ± 0.1	7.470	60	85
Fe Kα	6.43 ± 0.01	6.403	1100	1200
Ca Kα	3.75 ± 0.07	3.690	45	45
Ar Kα	2.95 ± 0.06	2.957	65	55
S Kα	2.33 ± 0.05	2.307	140	165
Si Kα	1.75 ± 0.05	1.740	200	230

detectors and *XMM–Newton* mirrors. Similar structure is seen in the MOS spectrum and we proceed to study the MOS data in more detail, since here the statistics are comparable to the pn camera while the energy resolution is better. [The 1σ resolution of the MOS at the time of the Mkn 3 observation was ~34 eV at 1.5 keV (M. Kirsch, XMM-SOC-CAL-TN-0018 issue 2.3, 2004 July 28)].

Closer examination of the low-energy excess in the MOS spectrum confirms that the neutral Kα lines of Si, S, Ca and (probably) Ar are detected (Fig. 7). Table 1 compares the parameters of these lines, determined in XSPEC, with their laboratory energies and also with predicted equivalent widths for a cold solar abundance reflector (Matt, Fabian & Reynolds 1997). The general agreement of observed and predicted line strengths in Table 1 is very good and provides further support for the reflection-dominated description of the hard X-ray continuum of Mkn 3.

In addition to revealing several fluorescent lines, the MOS spectrum of Mkn 3 clearly resolves the principal resonance emission lines of highly ionized ions of Si and S, as well as of Mg, Ne and O. The unusual richness of the EPIC spectral data at these low energies is a consequence of the strong continuum source being hidden from direct view in Mkn 3. We examine this same spectral band with the higher-resolution RGS data in Section 4.

4 SPECTRAL LINES IN THE RGS DATA

The EPIC pn and MOS spectra of Mkn 3 show a 'soft excess' below ∼3 keV which contains both fluorescent emission from relatively cold matter and resonance line emission from highly ionized gas. We provisionally associate the latter with the extended soft X-ray emission resolved in the *Chandra* observation of Mkn 3 (Sako et al. 2000). To better quantify the soft X-ray spectrum of Mkn 3 we now examine the simultaneous *XMM–Newton* grating data.

We find the soft X-ray spectrum of Mkn 3 appears to be very similar to that of another nearby Seyfert 2 galaxy NGC 1068 (Kinkhabwala et al. 2002), being dominated by line emission from highly ionized stages of the lighter metals. Unfortunately, the fluxes are an order of magnitude less, mainly due to Mkn 3 lying at a greater distance, but also being significantly attenuated at the longer wavelengths by the relatively large Galactic column in the direction of Mkn 3. Nevertheless, visual examination of the RGS spectrum does allow the main properties of an ionized outflow to be determined, adding to the picture reported by Sako et al. (2000).

Figs 8–11 display the fluxed, background-subtracted RGS spectrum, combining both RGS-1 and RGS-2 data sets. The data are binned at 40 mÅ, comparable to the intrinsic resolution of the RGS. It is immediately evident that the spectrum is dominated by line emission and – except perhaps at the shortest wavelengths – the continuum level is low, consistent with the weak, unabsorbed power-law component in the EPIC spectral fit.

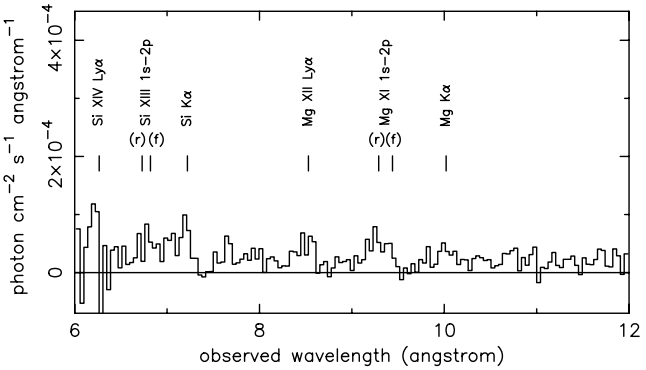

Figure 8. Fluxed RGS spectrum of Mkn 3 over the waveband 6–12 Å, binned at 40 mÅ and showing emission lines identified with ionized and neutral Si and Mg.

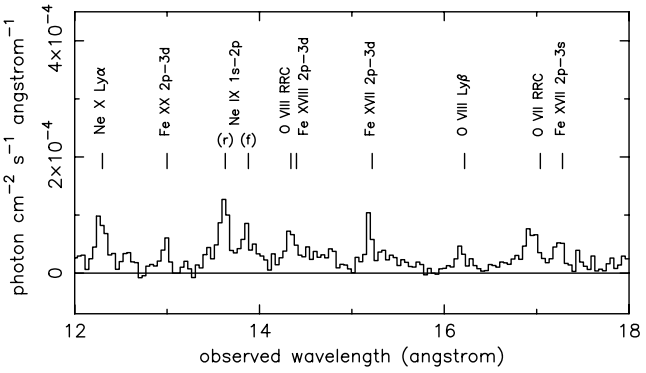

Figure 9. Fluxed RGS spectrum of Mkn 3 over the waveband 12–18 Å showing emission lines identified with ionized Ne, O and Fe, as well as RRC of O VII and O VIII.

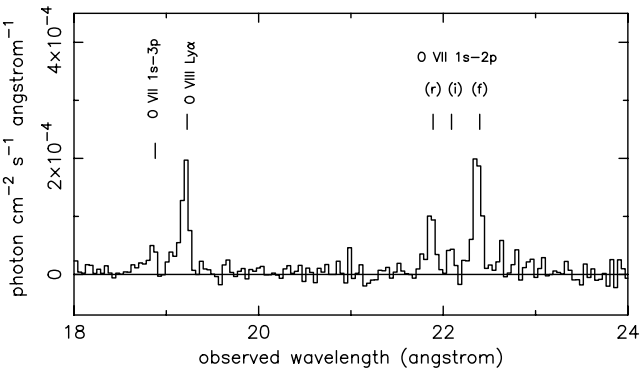

Figure 10. Fluxed RGS spectrum of Mkn 3 over the waveband 18–24 Å showing emission lines identified with O VIII Lyα and the O VII triplet.

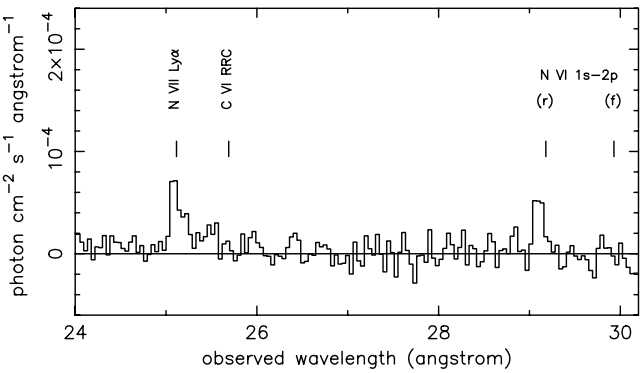

Figure 11. Fluxed RGS spectrum of Mkn 3 over the waveband 24–30 Å with emission lines identified with ionized N and C, together with a weak RRC of C VI.

4.1 An emission-line spectrum from a highly ionized gas

The shortest-wavelength sections of the RGS spectrum overlap that resolved by the MOS camera and find good qualitative agreement for the main emission lines of S, Si and Mg. Furthermore, the MOS identifications of the strong 0.9 keV feature – and the smaller peak near 1 keV – with the resonance lines of Ne IX and Ne X, respectively, are supported by the higher-resolution grating spectra.

Taken overall the RGS spectrum is characteristic of a recombining photoionized gas. The strongest emission lines are identified with resonance transitions in He- and H-like ions of the most abundant elements for this waveband, namely Si, Mg, Ne, O and N. The relative weakness of Fe-L emission, together with the detection of the narrow radiative recombination continuum (RRC) of O VII, O VIII and probably of C VI, indicates the gas is relatively cool ($kT \sim 6$ eV) and collisional ionization/excitation is unimportant.

Marked on Figs 8–11 are the laboratory wavelengths of the identified lines (adjusted for the redshift of Mkn 3), showing that the observed lines are generally shifted towards the blue. Table 2 lists the observed wavelengths and fluxes of the principal lines.

To better quantify the blueshift of the emission lines and also to derive other parameters of the emitting plasma, we fitted Gaussians

Table 2. Principal emission lines identified in the RGS spectrum of Mkn 3. Wavelengths are in Angstroms and adjusted to the source rest frame while line fluxes are in units of 10^{-6} photon cm^{-2} s^{-1}. The ionization parameter corresponds to that giving a maximum abundance of the relevant ion calculated for an optically thin gas irradiated by a $\Gamma = 1.8$ power law using XSTAR.

Line	λ_{source}	λ_{lab}	Flux	logξ
Si XIV Lyα	6.16 ± 0.04	6.18	8 ± 2	2.6
Si XIII 1s–2p (r)	6.62 ± 0.07	6.65	4 ± 2	2.1
Si XIII 1s–2p (f)	6.71 ± 0.05	6.74	6 ± 2	2.1
Si Kα	7.11 ± 0.03	7.13	10 ± 2	–
Mg XII Lyα	8.39 ± 0.05	8.42	8 ± 3	2.3
Mg XI 1s–2p (r)	9.14 ± 0.03	9.17	7 ± 2	2.0
Mg XI 1s–2p (f)	9.27 ± 0.05	9.31	5 ± 2	2.0
Mg Kα	9.87 ± 0.04	9.89	5 ± 2	–
Ne X Lyα	12.11 ± 0.03	12.13	9 ± 2	2.0
Fe XX 2p–3d	12.83 ± 0.02	12.84	4 ± 2	2.4
Ne IX 1s–2p (r)	13.43 ± 0.03	13.45	8 ± 2	1.5
Ne IX 1s–2p (f)	13.68 ± 0.05	13.70	6 ± 2	1.5
Fe XVII 2p-3d	14.98 ± 0.04	15.01	7 ± 2	1.8
O VIII Lyβ	15.97 ± 0.03	16.01	5 ± 1	1.6
Fe XVII 2p–3s	17.03 ± 0.03	17.06	7 ± 2	1.8
O VII 1s–3p	18.60 ± 0.03	18.63	5 ± 1	1.0
O VIII Lyα	18.940 ± 0.005	18.969	22 ± 3	1.6
O VII 1s–2p (r)	21.570 ± 0.007	21.602	9 ± 2	1.0
O VII 1s–2p (i)	21.78 ± 0.04	21.80	4 ± 1	1.0
O VII 1s–2p (f)	22.058 ± 0.005	22.095	22 ± 4	1.0
N VII Lyα	24.77 ± 0.03	24.78	9 ± 2	1.3
N VI 1s–2p (r)	28.71 ± 0.05	28.80	8 ± 3	0.7

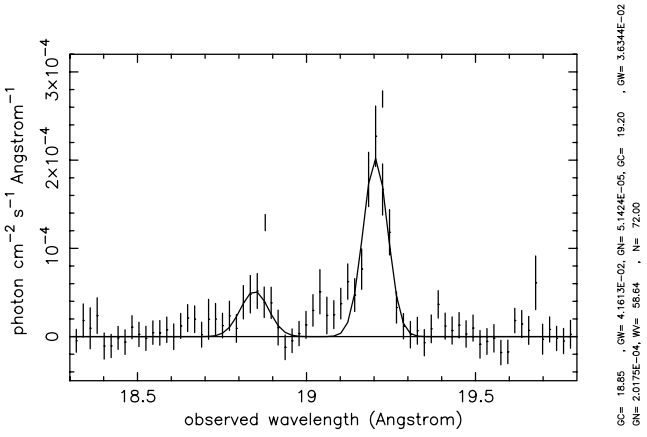

Figure 12. Fluxed RGS spectrum of Mkn 3, binned at 20 mÅ, with Gaussian fits to the 1s–3p emission of O VII and the Lyα line of O VIII.

to the fluxed spectra, now binned at 20 mÅ, for the strong O VII triplet and the O VIII Lyα line (Figs 12 and 13). The measured blueshifts are: O VII-r (0.032 ± 0.007 Å), O VII-f (0.037 ± 0.005 Å) and O VIII (0.029 ± 0.005 Å), corresponding to line-of-sight velocities of 440 ± 95, 500 ± 70 and 450 ± 75 km s^{-1}, respectively.

Assuming a common Gaussian profile for the above lines yielded an observed width of 85 ± 11 mÅ (FWHM). Allowing for the RGS1 resolution of 60 ± 5 mÅ (FWHM), we find the O VII and O VIII emission lines are broadened by 60 ± 12 mÅ (FWHM). Assuming velocity broadening that corresponds to a velocity dispersion of 900 ± 180 km s^{-1}.

In the O VII triplet (Fig. 12) the forbidden line is significantly stronger than the resonance line, with the intercombination lines being relatively weak. While it is possible – perhaps probable – that the resonance line in O VII is affected by core absorption (see Section 5.2) the strong forbidden line is consistent with emission from a photoionized gas in 'the low-density regime', namely $n_e \leqslant 10^{10}$ cm^{-3} (Porquet & Dubau 2000). We discuss other information that can be deduced from the well-determined O VII triplet in Section 5.2.

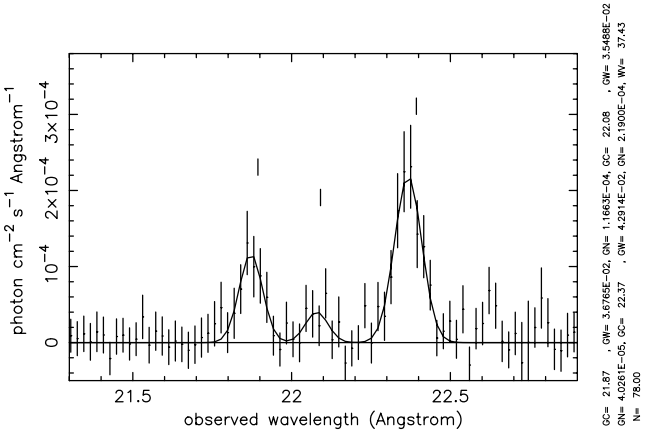

Figure 13. Fluxed RGS spectrum of Mkn 3 with Gaussian fits to the resonance, intercombination and forbidden lines of O VII.

The suggestion of a 'blue wing' to many of the stronger emission lines is interesting. This is most noticeable for O VIII Lyα (Fig. 13), where there is no competing line blend, but can also be seen in the resonance lines of O VII and Ne IX. If interpreted as a higher velocity component to the relevant emission line, the corresponding projected outflow velocity would be ∼3000 km s^{-1}. We return to this possibility in Section 6.

5 DISCUSSION

5.1 A reflection-dominated hard X-ray spectrum

Our analysis of the EPIC data confirms and refines the model proposed by Turner et al. (1997a) and later adopted by Cappi et al. (1999) in their respective analyses of *ASCA* and *BeppoSAX* observations of Mkn 3. The improved quality of the EPIC spectra are significant in several respects. First, observing the hard X-ray spectrum to ∼15 keV allows the absorbed power-law and reflection components to be separated and quantified, for the first time within a single data set. This confirms Mkn 3, one of the brightest AGN in the hard X-ray sky, to have an intrinsic power-law continuum typical of a Seyfert 1 nucleus, but attenuated by a near-Compton-thick absorber of cold matter, resulting in the observed X-ray radiation at ∼3–8 keV being dominated by cold reflection. Secondly, the fluorescence line emission of all abundant elements from Ni to Si (and possibly Mg) are detected, consistent with the reflection-dominated model. Thirdly, the Fe Kα line is sufficiently well determined to indicate a small but significant 'blueshift'. We find no evidence for an absorption edge at ∼8.4 keV reported in an independent analysis of the *ASCA* data by Griffiths et al. (1998). Conversely, the edge energies for both the absorber and reflector lie close to 7.1 keV, appropriate to near-neutral Fe.

Removing the pn double-pixel counts, and including a Compton shoulder, reduces the apparent width of the Fe Kα line in the pn data to a 'marginally resolved' $\sigma = 32 \pm 15$ eV. Allowing for the Compton shoulder in the MOS fit makes the linewidth similarly marginal. However, inclusion of the Compton scattered component

increases the energy of the primary line, which now lies in the range 6.43 ± 0.01 keV (at the redshift of Mkn 3) in both pn and MOS data, compared with a laboratory energy (weighted mean of Kα_1 and Kα_2) of 6.40 keV. With an absolute error of ∼5 eV for the MOS and ∼10 eV for the pn camera (XMM-SOC-CAL-TN-0018), we conclude that the line is 'blueshifted' by 30 ± 10 eV. If that shift were due to the ionization state of the reflecting matter it would correspond to Fe XV–XVIII (House 1969); however, that would show the Fe K edge energy to be $\gtrsim$7.5 keV, in conflict with the value observed. The most obvious alternative is a velocity shift with a projected (line-of-sight) velocity of 3200 ± 1100 km s^{-1}. We note that neither the line energy nor the (marginally resolved) linewidth of Fe Kα in Mkn 3 sit comfortably with cold reflection from the unobscured far-side inner wall of the putative molecular torus. Interestingly, Iwasawa et al. (1994) also found a blueshifted Fe Kα line in the *ASCA* spectrum, and, furthermore, claimed the line flux to vary over a 3.5-yr interval. Griffiths et al. (1998) also concluded that the Fe Kα line flux fell by a factor of ∼1.8 between *Ginga* and *ASCA* observations in 1989 and 1993. On the other hand, Sako et al. (2000) reported a Kα line at 6.391 ± 0.004 keV (before allowing for any Compton shoulder) from an early *Chandra* High Energy Transmission Grating (HETG) observation, with a width of ∼36 ± 4 eV.

Taken overall, the form of the 'cold' reprocessor indicated by the EPIC spectra is unclear. The strong reflection continuum and ∼1 keV EW Fe Kα line match well with an origin in the exposed far inner wall of a torus, the near side of which forms the absorbing barrier to the primary power-law source. However, the observed Fe Kα line energy – and a similar blueshift of the Fe K edge in the absorber – suggests a significant part of the fluorescent emission may arise in cold, dense 'clouds' in the same 'near-side' outflow that also obscures the continuum source from direct view in Mkn 3.

5.2 Extended photoionized gas in Mkn 3

The RGS spectrum of Mkn 3 is dominated by narrow emission lines and RRC of highly ionized gas. The agreement with the *Chandra* observation reported by Sako et al. (2000) is good, consistent with the conclusion of those authors that both photoionization/recombination and photoexcitation/radiative emission are important in the soft X-ray spectrum of Mkn 3. While not affecting that basic conclusion, the independent determination of line energies and fluxes with the RGS is useful, given the low count rates in both observations. The characteristics of the RGS and *Chandra* HETG are also complementary, with the former having higher sensitivity for the important O VII and O VIII lines (with ∼100–200 counts per line) while the HETG extends the high-resolution spectrum to much higher energies. The RGS data longward of ∼12 Å show the underlying continuum to be negligible, consistent with the broad-band EPIC fit (e.g. Fig. 3) which includes a (maximum) power-law component of ∼1 per cent of the intrinsic power law. If electron scattering from the (optically thin) ionized outflow produces the polarized broad emission lines seen in the optical spectrum of Mkn 3 (Miller & Goodrich 1990; Tran 1995), our upper limit to the unabsorbed power-law component constrains the product $C\tau$ to be $\leqslant$0.01, where C is the covering factor of the ionized outflow and τ is its optical depth in the line of sight.

Further information on the ionized gas can be obtained from the emission-line spectrum. The observed intensity of the forbidden (22.1-Å) line of O VII is a useful measure, since it is unaffected by resonance absorption. Assuming a solar abundance of oxygen, with 25 per cent in O VII, 50 per cent of recombinations from O VIII direct to the ground state and a recombination rate at $kT \sim 6$ eV (from the corresponding RRC width) of 10^{-11} cm^3 s^{-1} (Verner & Ferland 1996), we estimate an emission measure of the order of 1.5×10^{64} cm^{-3}. The ion species listed in Table 2 suggest the coexistence of gas over a wide range of ionization, yielding a total emission measure a factor of several higher. The extent of the emission region is not directly constrained by the line intensities or the ionization parameter, but given the Seyfert 2 nature of Mkn 3 a reasonable minimum radius is $r \sim 1$ pc (3×10^{18} cm). With the emission volume approximated by a cylinder of radius r and length $10r$, a uniform density gas would then have $n_e \sim 4 \times 10^3$ cm^{-3}.

The ionization parameter ξ ($= L/nr^2$) provides a check on those simple estimates, where L is the (unabsorbed) X-ray continuum flux irradiating the outflow. The EPIC spectral fit found L ($\gtrsim$0.3 keV) ∼ 2.6×10^{43} erg s^{-1}, giving an ionization parameter of $\xi \sim 30$ cm^{-1} at $r = 5$ pc, a value at which O VII and O VIII would both be prominent. In fact, the detection of He-like N VI and H-like Si XIV in the RGS spectrum shows the emitting gas must cover a wide range of ionization parameter, those ions having peak abundances at ξ of ∼5 and ∼400. Assuming the ionized S and Ca emission lines detected in the MOS spectrum arise in the same outflow requires still more highly ionized gas, while the excess flux in the EPIC data at ∼6.6–6.8 keV, if correctly attributed to emission from Fe XXV, extends that range to ξ of ∼1000. Such a broad ionization structure, where the distance to the ionizing source is constrained to $r \gtrsim r_{\rm BLR}$, suggests an inhomogeneous gas with a correspondingly broad range of density. While the present spectra are clearly inadequate to allow such a complex ionized outflow to be mapped it is possible to estimate several additional parameters.

Line ratios in the He-like triplet are an established diagnostic of ionized plasmas. In the RGS spectrum of Mkn 3 the O VII triplet is well defined, with the forbidden (f), resonance (r) and intercombination (i) lines all detected (Fig. 12). The observed line strengths are in the ratio 22:9:4, yielding values of the diagnostic parameters R ($= f/r + i$) ∼ 5 and G ($= f + i/r$) ∼ 3, which are rather high and low, respectively, compared with the calculated ratios for a pure, low-density photoionized plasma (Porquet & Dubau 2000). More recent calculations, which take account of the column density and the ionization parameter in the radiating gas (Godet, Collin & Dumont 2004), yield $G = 3$ for O VII for a column density of the order of $N_{\rm H} \sim 10^{21-22}$ cm^{-2} and $\xi = 30$–100. Encouragingly, that column is of the same order as the product n_er in the above simple fit to the calculated emission measure, and also to the estimated scattering τ for a covering factor of 0.1. In particular, the resonance line of O VII (21.6 Å) will be optically thick in the core, limiting the effects of photoexcitation in comparison with higher-order lines. We note also that the f:r line ratios are lower in the Ne and Mg triplets, suggesting the opacity effects there are less.

The mass of the (observed) extended gas envelope is ∼900 M$_\odot$, assuming a uniform density. With a projected outflow velocity, at ∼45° to the line of sight, of ∼700 km s^{-1}, the mass outflow rate is then ∼0.04 M$_\odot$ yr^{-1}, with an associated mechanical energy of 2×10^{40} erg s^{-1}. These estimates would be reduced if the emitting gas were indeed clumpy.

From the absorption-corrected 2–10 keV luminosity of 1.5×10^{43} erg s^{-1} we estimate a bolometric luminosity for Mkn 3 of 4×10^{44} erg s^{-1}. At an accretion efficiency of 0.1 the accretion mass rate is then ∼0.06 M$_\odot$ yr^{-1}. Thus, as may generally be the case in Seyfert 1 galaxies, we find the ionized outflow in Mkn 3 carries a significant mass loss from the AGN. However, at least by a radial distance $r \gtrsim r_{\rm BLR}$, the kinetic energy in the outflow is relatively small, even compared with the soft X-ray luminosity.

6 CONCLUSIONS

XMM–Newton EPIC observations of high statistical quality confirm previous findings that the extremely hard (2–10 keV) power-law index in the Seyfert 2 galaxy Mkn 3 is due to strong continuum reflection from 'cold' matter. The intrinsic power law, which is seen through a near-Compton-thick absorber, emerges above ∼8 keV and has a photon index typical of Seyfert 1 galaxies. The dominant reflection component in Mkn 3 appears to be unaffected by the large absorbing column, allowing fluorescent line emission to be detected from Ni Kα (∼7.5 keV) down to Mg Kα (∼1.25 keV).

The combination of a large column density obscuring the continuum source with the visibility of a large area of cold reflector suggests that Mkn 3 is being viewed at an inclination which cuts the edge of the obscuring screen. This would be consistent with the geometry of 'Seyfert galaxies on the edge', identified in a recent extensive review of the optical polarization properties of Seyfert galaxies (Smith et al. 2002, 2004). Comparison with the *XMM–Newton* spectrum of NGC 4151 (e.g. Schurch et al. 2003) suggests that the well-studied Seyfert 1 galaxy may be inherently similar but is being viewed from the other (lower obscuration) side of a (blurred) edge.

The strong Fe Kα line appears to be 'blueshifted' in both EPIC pn and MOS spectra, indicating an origin in low-ionization matter with a projected outflow velocity of 3100 ± 1100 km s^{-1}. Although less well resolved after the inclusion of a Compton shoulder, the Fe Kα line has a formal width of 3200 ± 1600 km s^{-1} (FWHM). The projected velocity and indicated velocity dispersion are both inconsistent with an origin at the far inner wall of a torus of $r \gtrsim 1$ pc. It seems more likely that a large fraction of the neutral Kα emission arises in dense matter circulating or outflowing at a radial distance more typical of the BLR clouds. For comparison, we note that Tran (1995) found the FWHM of Hβ in polarized light to be 6000 km s^{-1}.

Below ∼3 keV a 'soft excess' emerges above the hard, reflection-dominated continuum. Spectral structure is resolved in both EPIC and RGS data, with the MOS spectrum showing remarkable detail. In this soft X-ray band the spectrum is found to be dominated by resonance lines of He- and H-like Si, Mg, Ne, O and N, with an observed blueshift of 470 ± 70 km s^{-1}, indicating an origin in a highly ionized outflow extending above the Seyfert 2 absorbing screen.

Relative line fluxes and the detection of narrow (low-temperature) radiative recombination continua of O VII, O VIII and (probably) C VI are all consistent with the gas being photoionized/photoexcited by the intrinsic power-law continuum, as found by Sako et al. (2000). In all of these respects the soft X-ray-emitting gas in Mkn 3 is very similar to that seen in another nearby, and still brighter, Seyfert 2 galaxy NGC 1068 (Kinkhabwala et al. 2002). As those authors pointed out, the ionized outflow seen in emission in NGC 1068 – and in Mkn 3 – is consistent with that typically seen in absorption against the power-law continuum in Seyfert 1 galaxies. The soft X-ray luminosity in Mkn 3 is of the order of 1 per cent of the intrinsic (absorption-corrected) 0.3–10 keV luminosity.

It is interesting to compare that figure with the 'non-varying' component of the soft X-ray excess found in the Seyfert 1 galaxies NGC 4051 (Pounds et al. 2004a) and 1H0419-577 (Pounds et al. 2004b), where soft X-ray luminosities of 5 and 9 per cent of the dominant power-law component were indicated. It was suggested in those papers that a large part of the non-varying soft flux might be explained by the same outflow usually seen in absorption. For that explanation to hold up it would appear that a bright inner region, shielded from direct view in a Seyfert 2 such as Mkn 3, must have a sufficiently high velocity dispersion to remain undetected in high-resolution absorption spectra. Interestingly, Gierlinski and Done outlined an extreme case of such a scenario in proposing an absorption-based alternative to the strong soft excess in the luminous Seyfert 1 galaxy PG1211+577 (Gierlinski & Done 2004). The blue wings seen on some of the stronger emission lines in the RGS spectrum may be an indication of such a trend to higher-velocity gas extending into the unobscured outflow in Mkn 3. However, significant emission could come from a second ionized emission component out of the line of sight to the continuum source (and hence not seen in absorption in Seyfert 1s) within the cone of the obscuring torus. Such a component might be identified with the 'equatorial scatterer' required by optical polarization studies of Seyfert galaxies (Smith et al. 2002, 2004).

ACKNOWLEDGMENTS

The results reported here are based on observations obtained with *XMM–Newton*, an ESA science mission with instruments and contributions directly funded by ESA Member States and the USA (NASA). The authors wish to thank Leicester colleagues for valuable input, the SOC and SSC teams for organizing the *XMM–Newton* observations and initial data reduction. KAP acknowledges the support of a Leverhulme Trust Emeritus Fellowship and KPA of a PPARC research grant.

REFERENCES

Arnaud K. A., 1996, ASP, Conf. Ser. 101. Astron. Soc. Pac., San Francisco, p. 17
Capetti A., Machetto F., Axon D. J., Sparks W. B., Boksenberg A., 1995, ApJ, 448, 600
Capetti A., Axon D. J., Machetto F., Marconi A., Winge C., 1999, ApJ, 516, 187
Cappi M. et al., 1999, A&A, 344, 857
den Herder J. W. et al., 2001, A&A, 365, L7
Gierlinski M., Done C., 2004, MNRAS, 349, L7
Godet O., Collin S., Dumont A. M., 2004, A&A, 426, 267
Griffiths R. G., Warwick R. S., Georgantopoulos I., Done C., Smith D. A., 1998, MNRAS, 298, 1159
House L. L., 1969, ApJS, 18, 21
Iwasawa K., Yaqoob T., Awaki H., Ogasaka Y., 1994, PASJ, 46, L167
Kallman T., Liedahl D., Osterheld A., Goldstein W., Kahn S., 1996, ApJ, 465, 994
Kaspi S. et al., 2002, ApJ, 574, 643
Kinkhabwala A. et al., 2002, ApJ, 575, 732
Magdziarz P., Zdziarski A. A., 1995, MNRAS, 273, 837
Matt G., 2002, MNRAS, 337, 147
Matt G., Fabian A. C., Reynolds C. S., 1997, MNRAS, 289, 175
Miller J.S., Goodrich R. W., 1990, ApJ, 355, 456
Nandra K., Pounds K. A., 1994, MNRAS, 268, 405
Nandra K., Pounds K. A., Stewart G. C., Fabian A. C., Rees M. J., 1989, MNRAS, 236, 39
Pogge R. W., de Robertis M. M., 1993, ApJ, 404, 563
Porquet D., Dubau J., 2000, A&A, 143, 495
Pounds K. A., Reeves J. N., King A. R., Page K. L., 2004a, MNRAS, 350, 10
Pounds K. A., Reeves J. N., Page K. L., O'Brien P. T., 2004b, ApJ, 616, 696
Sako M., Kahn S. M., Paerels F., Liedahl D. A., 2000, ApJ, 543, L115
Schurch N. J., Warwick R. S., Griffiths R. E., Sembay S., 2003, MNRAS, 345, 423
Smith J. E., Young S., Robinson A., Corbett E. A., Giannuzzo M. E., Axon D. J., Hough M. H., 2002, MNRAS, 335, 773

Smith J. E., Robinson A., Alexander D. M., Young S., Axon D. J., Corbett E. A., 2004, MNRAS, 350, 140
Stark A. A., Gammie C. F., Wilson R. W., Bally J., Linke R., Heiles C., Hurwitz M., 1992, ApJS, 79, 77
Strüder L. et al., 2001, A&A, 365, L18
Tifft W. G., Cocke W. J., 1988, ApJS, 67, 1
Tran H. D., 1995, ApJ, 440, 565
Turner M. J. L. et al., 2001, A&A, 365, L27
Turner T. J., George I. M., Nandra K., Mushotzky R. F., 1997a, ApJ, 488, 164
Turner T. J., George I. M., Nandra K., Mushotzky R. F., 1997b, ApJS, 113, 23
Verner D. A., Ferland G. J., 1996, ApJS, 103, 467

This paper has been typeset from a TEX/LATEX file prepared by the author.